Wireless Personal Communications (2023) 133:1963–1985
https://doi.org/10.1007/s11277-023-10837-y

Re-configurable Intelligent Surfaces Assisted Simultaneous Wireless Information and Power Transfer

Fang-Biau Ueng[1] · Hsuan-Fu Wang[2] · Huang-Wei Shen[1]

Accepted: 21 December 2023 / Published online: 9 February 2024

Abstract
The bandwidth limitation is an arduous challenge to deploy the large-scale Internet of Things (IoTs) beyond fifth-generation (B5G) communication networks. Although the millimeter wave (mmWave) technology can provide greater bandwidth at the cost of complex processors in harsh environments, it can be a solution to establish large-scale IoTs. Still, its cost and power requirements become obstacles to widespread adoption. In this context, Reconfigurable Intelligent Surfaces (RISs) can be a crucial technology to meet this challenge. In this paper, we study the B5G RIS-assisted MIMO simultaneous wireless-information and power-transfer (SWIPT) mmWave large-scale IoTs, where active BS transmitted beamformer and passive RIS reflection vector are jointly optimized to maximize the minimum signal-to-interference-plus-noise-ratio (SINR) of all the information decoders (ID) and the minimum harvested power of all the energy receivers (ER) is maintained. The simulation result demonstrates the effectiveness of the proposed system.

Keywords mmWave · Reconfigurable Intelligent Surfaces · Simultaneous wireless information · Power transfer

1 Introduction

Driven by economic and environmental issues, the design of energy-efficient high-bandwidth wireless communication technology has become critical [1]. In this paper, the joint development of the millimeter-wave (mmWave) spectrum, which can provide high bandwidth, and Reconfigurable Intelligent Surfaces (RIS), which can reduce energy usage, has the potential to achieve this goal. The low-power, low-throughput nature of routinely deployed IoT devices has led to neglecting such high-frequency bands with rather severe propagation characteristics when building IoT environments. However, the emergence of large-scale IoT applications has spawned a large number of devices, putting pressure on low-bandwidth technologies below 6 GHz, and mmWave has emerged as a candidate solution for quasi-scenarios such as smart grids, smart cities, and intelligent industries [2]. The

✉ Fang-Biau Ueng
fbueng@nchu.edu.tw

1 Department of Electrical Engineering, National Chung-Hsing University, Taichung, Taiwan

2 Department of Aeronautical Engineering, National Formosa University, Yunlin, Taiwan

main challenge in this situation is that mmWave transceivers typically employ digital or hybrid beamforming, with multiple RF chains and numerous antenna arrays that can focus electromagnetic energy to specific angles to counter the high attenuation characteristic of the mmWave. However, it becomes infeasible when this approach is used for power-constrained IoT devices because multiple active devices consume energy [3]. For such problems and challenges, RIS can be a solution by exploiting the vast bandwidth resources of mmWave while allowing advanced large-scale IoT scenarios with an extremely low probability of service interruption [4]. RIS utilizes controllable transformations to incoming radio waves without power amplifiers, creating many possible solutions for optimizing low-cost, low-energy wireless systems [5]. RIS has acquired much attention [6–21] due to its ability to transform the random nature of the wireless environment into a programmable channel that has an active role in how the signal propagates. RIS has been proposed for various applications, including secure communications [15, 16], non-orthogonal multiple access [17], wireless computing [18], or energy-efficient cellular networks [19, 20]. RIS is a continuous meta-surface modeled as a grid of discrete unit cells separated by subwavelength distances that can programmatically change its electromagnetic response (such as phase, amplitude, polarization, and frequency). For example, they can be adjusted so that the signals bouncing off the RIS are combined constructively to improve the signal quality at the intended receiver end or destructively to avoid signal leakage to undesired receivers. Conceptually, RIS may raise some of the challenges behind traditional amplify-and-forward (AF) relay methods [22] and beamforming methods used in (massive) MIMO [23]. There are significant differences between conventional AF relays and RIS [24, 25]. The former relies on active low-noise power amplifiers and other active electronic components such as DAC or ADC converters, mixers, and filters. In contrast, RIS has a shallow hardware footprint and consists of one or a few layers of planar structures that can be built using photolithographic or nanoimprinting methods. Therefore, RIS is particularly attractive for seamless integration into walls, ceilings, object boxes, architectural glass, and clothing [26].

On the other hand, (massive) MIMO uses many antennas to obtain significant beamforming gains. In fact, under similar conditions, massive MIMO and RIS techniques can produce equal signal-to-noise ratio (SNR) profits. However, RIS passively achieves this beamforming gain. In this paper, active beamforming through the transmitter antenna array and passive beamforming through the RIS in the channel can compensate for each other and provide more significant gain when both are optimized together, which is precisely the goal of this paper. Although massive MIMO technology can significantly improve the efficiency of wireless information transfer (WIT) and wireless power transfer (WPT) in emerging IoT networks by exploiting the gain of large arrays, this usually comes at a high cost [27–29]. As a remedy, radio frequency (RF) chains can be used in so-called hybrid implementations than transmit/receive antennas. This can also result in high hardware costs, high signal processing overhead, and high energy consumption, hindering implementation. As a cost-effective alternative to massive MIMO technology, RIS enables unprecedented spectral and energy efficiency, especially in complex propagation scenarios with severe signal blocking. However, because RIS is a reconfigurable metal surface with many passive reflective elements, it cannot perform as complex signal processing as large arrays and active MIMO repeaters. It is usually served with lower hardware costs and low power consumption. By adjusting the phase shift and amplitude attenuation of each RIS reflective element, an excellent wireless propagation environment can be actively constructed for WIT and WPT [30, 31]. Because of the above advantages, research on RIS-assisted communication for various wireless systems such as MISO systems [32, 33], point-to-point MIMO systems [34], multicell multiuser MIMO systems [35], and MIMO-OFDM systems [36, 37] attracted attention. These studies usually assume perfect channel state information (CSI). Traditional training-based channel estimation schemes cannot be directly applied due to the lack of fundamental frequency processing capability of RIS operating without RF chains and the need to estimate many RIS-related channels. As an alternative, under the assumption of uplink-downlink channel reciprocity for flat frequency channels and frequency selective channels, various channel estimation schemes using RIS grouping strategies have been proposed previously [36–41].

Nonetheless, there are new challenges to integrating RF energy harvesting and advanced WIT technologies for sustainable green IoT networks. To this end, Simultaneous Wireless Information and Power Transfer (SWIPT) has been evaluated as an attractive, innovative technology [42]. Recently, there has been increasing interest in RIS-based SWIPT systems [9, 43–45]. For example, [43] studied weighted harvested energy maximization in a RIS-assisted MISO SWIPT system and demonstrated that dedicated energy beamforming is practically optional. As a further development, the maximization of the minimum harvested energy among all energy receivers (ERs) in this system is studied from a fairness perspective [44]. By deploying multiple RIS, [45] investigated total transmit power minimization subject to separate QoS constraints at the Information Decoder (ID) and ER. Pan et al. [35] considered a more general RIS-assisted MIMO SWIPT system and studied the weighted sum rate maximization of all IDs while guaranteeing a particular minimum total harvested energy across all ERs. Various advanced communication technologies in IoT networks, such as NOMA [46, 47], Physical Layer Security [48, 49], and Mobile Edge Computing (MEC), have also been integrated with this technology. RIS achieves better system performance, so in this paper, we consider a RIS-assisted MIMO SWIPT system consisting of a multi-antenna base station (BS), a RIS to assist communication, and multiple SWIPT-enabled systems. It consists of several IoT devices, and RIS is deployed to assist SWIPT from the BS to these IoT devices. From a fairness perspective, we further investigate the maximization of the minimum SINR among all IDs by jointly optimizing the active BS transmit beamforming vector and the passive RIS reflection coefficient, premised on the minimum total harvested energy required for all ERs.

2 System Model and Problem Formulation

This section introduces the system model and problem description. We first present the entire system's architecture and then describe our goals and the problems.

As shown in Fig. 1, we consider a RIS-assisted wireless communication system in which the RIS is deployed to assist the multi-antenna APs in the SWIPT system. It is transmitted from the AP of M antennas to two parts, including the information user (IU) and energy user (EU); the number of IU is K_I, and the number of EU is K_ε. For simplicity, we consider linear transmit precoding at the AP and assume that each IU/EU is assigned a separate information/energy beam without loss of generality. Therefore, the transmission signal from the AP can be expressed as

$$x = \sum_{i \in K_I} w_i s_i^I + \sum_{j \in K_\varepsilon} v_j s_j^E, \tag{1}$$

where $w_i \in C^{M\times 1}$ is the precoding vector of IU, $v_j \in C^{M\times 1}$ is the precoding vector of EU, s_i^I represents the message-bearing signal, and s_j^E represents the energy signal. s_i^I are assumed to be independent and identically distributed signals with zero mean and variance one,

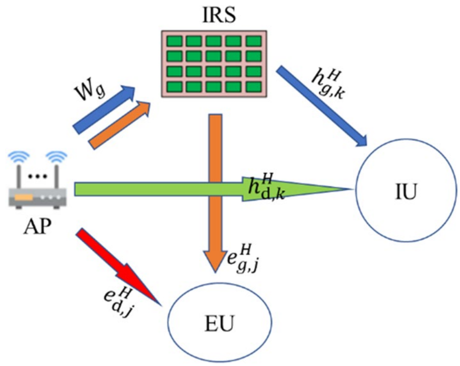

Fig. 1 System model

while s_j^E carry no information; they can be any random signals. Therefore, the total transmit power required by the AP is expressed as follows.

$$E\left(x^H x\right) = \sum_{i\in K_I} \|w_i\|^2 + \sum_{j\in K_\varepsilon} \|v_j\|^2, \tag{2}$$

Next is the part of the signal received by the IU, $h^H_{d,k} \in C^{1\times M}$ is the channel directly transmitted by the AP to the IU, $h^H_{g,k} \in C^{1\times L}$ is the channel that the RIS transmits to the IU, $e^H_{d,k}$ is the channel that the AP transmits directly to the EU, $e^H_{g,k}$ is the channel that the RIS sends to the EU, $W_g(l)$ indicates the channel transmitted from the AP to the RIS and $\Phi_g^H(l)$ represents the reflective element channel in the RIS. Since implementing independent control of reflection amplitude and phase is expensive, it is advantageous to design each element to maximize signal reflections for simplicity. Therefore, we express the signal received by the IU from AP to IU and AP to RIS and then to IU as the following equation:

$$y_k^I = \left(\sum_{l=1}^{L} h^H_{g,k}(l)\Phi_g^H(l)W_g(l) + h^H_{d,k} \right) x + \sigma_k, \tag{3}$$

where $\sigma_k \sim CN\left(0, \sigma_k^2\right)$ is an independent and identically distributed Gaussian noise, and we simplify Eq. (3) and rewrite it as (4):

$$y_k^I = \left(h^H_{g,k}\Phi_g^H W_g + h^H_{d,k} \right) x + \sigma_k, \tag{4}$$

where $h^H_{g,k} = \left[h^H_{g,k}(1), \ldots, h^H_{g,k}(L)\right]^T \in C^{N\times N}$, $W_g = \left[W_g(1), \ldots, W_g(L)\right]^T \in C^{N\times M}$, and $\Phi_g^H = \mathrm{Diag}\left(\Phi_g^H(1), \ldots, \Phi_g^H(L)\right) \in C^{N\times N}$.

Since the energy beam carries no information but a pseudo-random signal, its waveform can be assumed to be known at the AP and each IU before data transmission. We hypothesize that the interference they cause can be canceled at each IU, which contributes to the fundamental performance limitations of our SWIPT system and the study of the impact of RIS on energy beamforming. Therefore, we express SINR as Eq. (5):

$$SINR_k = \gamma_k = \frac{\left|\sum_{g=1}^{G} h_{g,k}^H \Phi_g^H W_g w_i\right|^2}{\sum_{k=1,k\neq i}^{K} \left|\sum_{g=1}^{G} h_{g,k}^H \Phi_g^H W_g w_k\right|^{2^2} + \sigma_i^2}. \tag{5}$$

On the other hand, it is part of the energy received by the EU. We express the energy received by the EU with Eq. (6):

$$Q_j = \sum_{i\epsilon K_i} \left|(e_{g,j}^H \Phi_g^H W_g + e_{d,j}^H) w_i\right|^2 + \sum_{i\epsilon K_\varepsilon} \left|(e_{g,j}^H \Phi_g^H W_g + e_{d,j}^H) v_m\right|^2. \tag{6}$$

Then comes the problem description part; our goal is to maximize the transmission rate of the entire system through optimization subject to the constraints of the transmission power and the energy harvesting at the EU. We formulate the problem description as Eq. (7):

$$\begin{aligned}
&\underset{P,\Phi_g}{Maximize} f_1\left(P,\Phi_g\right) = \sum_{k=1}^{K} z_k log_2\left(1+\gamma_k\right), \text{Subject to} \\
&\sum\nolimits_{i\in K_I} \left\|w_i\right\|^2 + \sum\nolimits_{\mathrm{j}\in K_\varepsilon} \left\|v_j\right\|^2 \le P, \\
&\sum\nolimits_{i\in K_i} \left|\left(e_{g,j}^H \Phi_g^H W_g + e_{\mathrm{d},j}^H\right) w_i\right|^2 + \sum\nolimits_{i\in K_\varepsilon} \left|\left(e_{g,j}^H \Phi_g^H W_g + e_{\mathrm{d},j}^H\right) v_m\right|^2 \ge E_j, \\
&0 < \theta_n \le 2\pi, \forall n \in N.
\end{aligned} \tag{7}$$

where z_k is the data weight assigned to the kth IU, P represents the maximum transmission power, $E_j > 0$ is the least energy received by each energy user, and θ_n represents the phase of the RIS.

3 The Proposed Method and Algorithm

First, we change the formula of power limit into the form of rank, such as Eq. (8):

$$\begin{aligned}
&\underset{P,\Phi_g}{maximize} f_1\left(P,\Phi_g\right) = \sum_{k=1}^{K} z_k log_2\left(1+\gamma_k\right), \text{Subject to} \\
&\sum\nolimits_{k\in K} Tr\left(W_k\right) + Tr\left(V_l\right) \le P, \\
&\sum_{i\in K_i} \left|\left(e_{g,j}^H \Phi_g^H W_g + e_{\mathrm{d},j}^H\right) w_i\right|^2 + \sum_{i\in K_\varepsilon} \left|\left(e_{g,j}^H \Phi_g^H W_g + e_{\mathrm{d},j}^H\right) v_m\right|^2 \ge E_j, \\
&0 < \theta_n \le 2\pi, \forall n \in N.
\end{aligned} \tag{8}$$

Next, we use the Lagrangian dual transformation (LDT) [29] that the term $\sum_{k=1}^{K} z_k log_2\left(1+\gamma_k\right)$ can be converted into $\sum_{k=1}^{K} z_k ln\left(1+\alpha_k\right) - z_k\alpha_k + \frac{z_k\left(1+\alpha_k\right)\gamma_k}{1+\gamma_k}$. Therefore, we transform f_1 into problem f_2, which is represented by Eq. (9):

$$\underset{P,\Phi_g,\alpha}{Maximize} f_2\left(P,\Phi_g,\alpha\right)=\sum_{k=1}^{K} z_k ln\left(1+\alpha_k\right)-z_k\alpha_k+\frac{z_k\left(1+\alpha_k\right)\gamma_k}{1+\gamma_k}, \text{Subject to} \\ tr\left(PP^H\right)\le P, \sum\nolimits_{i\in K_i}\left|e_j^H w_i\right|^2+\sum\nolimits_{i\in K_\varepsilon}\left|e_j^H v_m\right|^2\ge E_j, \text{and } \theta_{g,m}\in F_c,\forall g,\forall m, \tag{9}$$

where $\alpha=\left[\alpha_1,\cdots,\alpha_k\right]^T$ is the additional vector generated after conversion. Note that f_1 and f_2 are equivalent, so solving f_1 is equivalent to solving f_2. In addition, the formula of the transmission power is simplified again, and the mathematical symbol e_j^H is used to represent $e_j^H = e_{g,j}^H\Phi_g^H W_g + e_{\mathrm{d},j}^H$. After the conversion, we give α_k, optimize P and Φ_g, and rewrite the problem f_2 into the problem f_3 as follows,

$$\underset{P,\Phi_g}{maximize} f_3\left(P,\Phi_g\right)=\sum_{k=1}^{K}\frac{z_k\left(1+\alpha_k\right)\gamma_k}{1+\gamma_k} tr\left(PP^H\right)\le P, \text{ Subject to} \\ tr\left(PP^H\right)\le P, \sum\nolimits_{i\in K_i}\left|e_j^H w_i\right|^2+\sum\nolimits_{i\in K_\varepsilon}\left|e_j^H v_m\right|^2\ge E_j, \text{ and } \theta_{g,m}\in F_c,\forall g,\forall m. \tag{10}$$

Given the set $\left\{\Phi_1,\cdots,\Phi_g\right\}$ for convenience, we use the mathematical notation $\widetilde{h}_k^H$ to represent in Eq. (11):

$$\widetilde{h}_k^H=\sum_{g=1}^{G} h_{g,k}^H\Phi_g^H W_g. \tag{11}$$

Substitute Eq. (11) into Eq. (5), and rearrange f_3 to generate f_4, Eq. (12) is given as:

$$\underset{P}{Maximize} f_4(P)=\sum_{k=1}^{K}\frac{\overline{\alpha}_k\left|\widetilde{h}_k^H p_k\right|^2}{\sum_{j=1}^{K}\left|\widetilde{h}_k^H p_j\right|^2+\sigma_u^2}, \text{Subjectto} tr\left(PP^H\right)\le P, \tag{12}$$

where the symbol $\overline{\alpha}_k=z_k\left(1+\alpha_k\right)$, and we can see that f_4 is a multi-score programming problem, so we can use Quadratic Transform (QT) [29, 30] to convert f_4 to f_5, Eq. (13) is given as:

$$\underset{P,\beta}{maximize} f_5(P,\beta)=\sum_{k=1}^{K} 2\sqrt{\overline{\alpha}_k}\Re\left\{\beta_k^*\widetilde{h}_k^H p_k\right\}-\left|\beta_k\right|^2\left(\sum_{j=1}^{K}\left|\widetilde{h}_k^H p_j\right|^2+\sigma_u^2\right). \tag{13}$$

Note that $\beta=\left[\beta_1,\cdots,\beta_k\right]^T$ is the additional vector generated after the QT conversion in (13). To find the optimal solution of β_k, we need to calculate the partial derivative concerning β_k for (13) as follows:

$$\frac{\partial f_5}{\partial\beta_k}=2\sqrt{\overline{\alpha}_k}\widetilde{h}_k^H p_k-2\beta_k\left(\sum_{j=1}^{K}\left|\widetilde{h}_k^H p_j\right|^2+\sigma_u^2\right)=0. \tag{14}$$

$$\beta_k\left(\sum_{j=1}^{K}\left|\widetilde{h}_k^H p_j\right|^2+\sigma_u^2\right)=\sqrt{\overline{\alpha}_k}\widetilde{h}_k^H p_k. \tag{15}$$

$$\widehat{\beta}_k = \frac{\sqrt{\overline{\alpha}_k}\widetilde{h}_k^H p_k}{\sum_{j=1}^K \left|\widetilde{h}_k^H p_j\right|^2 + \sigma_u^2}. \tag{16}$$

Since the problem f_5 is a convex problem about p_k, using the Lagrange multiplier method, given β, the optimal solution of p_k can be described as Eq. (17):

$$\widehat{p}_k = \sqrt{\overline{\alpha}_k}\beta_k\left(\mu I_N + \sum_{i=1}^{k} |\beta_i|^2 \widetilde{h}_i \widetilde{h}_i^H\right)^{-1} \widetilde{h}_k \tag{17}$$

Next, we simplify the mathematical formula to facilitate the operation and derivation, $\widetilde{h}_k^H p_j$ can be expressed as Eq. (18):

$$\widetilde{h}_k^H p_j = \sum_{g=1}^{G} \theta_g^H diag\left(h_{g,k}^H\right) W_g p_j, \tag{18}$$

where $\boldsymbol{\theta}_g$ is defined as $\boldsymbol{\theta}_g = \left[\theta_{g,1}, \cdots, \theta_{g,M}\right]^T$ and $v_{g,k,j}$ is defined as $v_{g,k,j} = \text{diag}\left(h_{g,k}^H\right) W_g p_j$. Given α and P, we rewrite the problem f_4 into the problem f_6, as shown in Eq. (19):

$$\underset{\theta_g}{maximize} f_6\left(\theta_g\right) = \sum_{k=1}^{K} \frac{\overline{\alpha}_k \left|\sum_{g=1}^{G} \theta_g^H v_{g,k,k}\right|^2}{\sum_{j=1}^{K} \left|\sum_{g=1}^{G} \theta_g^H v_{g,k,j}\right|^{2^2} + \sigma_u^2},\ subject\ to$$
$$\left|\theta_{g,m}\right|^2 = 1, \forall g, \forall m \tag{19}$$

To facilitate the subsequent derivation, we first construct several symbols to represent the following equations, as shown in Eqs. (20) and (21):

$$\Theta = \left[\theta_1, \theta_2, \cdots, \theta_G\right]. \tag{20}$$

$$V_{k,j} = \left[v_{1,k,j}, v_{2,k,j}, \cdots, v_{G,k,j}\right]. \tag{21}$$

After the construction is completed, we can rewrite the problem f_6 into the problem f_7, as shown in Eq. (22):

$$\begin{aligned} \underset{\tilde{\theta}}{maximize} f_7\left(\tilde{\theta}\right) &= \sum_{k=1}^{K} \frac{\bar{\alpha}_k \left|tr\left(\Theta^H V_{k,k}\right)\right|^2}{\sum_{j=1}^{K} \left|tr\left(\Theta^H V_{k,j}\right)\right|^{2^2} + \sigma_u^2} \\ &= \sum_{k=1}^{K} \frac{\bar{\alpha}_k \left|\tilde{\theta}^H \tilde{v}_{k,k}\right|^2}{\sum_{j=1}^{K} \left|\tilde{\theta}^H \tilde{v}_{k,j}\right|^{2^2} + \sigma_u^2} \left|\theta_{g,m}\right|^2 \\ &= 1, \forall g, \forall m. \end{aligned} \tag{22}$$

Where $\tilde{\theta} = \text{vec}(\Theta)$, and $\widetilde{v}_{k,j} = \text{vec}\left(V_{k,j}\right)$. Next, we transform the problem f_7 into problem f_8 using quadratic transformation (QT) [29], as shown in Eq. (23):

$$\underset{\tilde{\theta},\rho}{maximize} f_8(\tilde{\theta},\rho) = \sum_{k=1}^{K} 2\sqrt{\overline{\alpha}_k}\Re\left\{\rho_k^*\tilde{\theta}^H\tilde{v}_{k,k}\right\} - \left|\rho_k\right|^2\left(\sum_{j=1}^{K}\left|\tilde{\theta}^H\tilde{v}_{k,j}\right|^2 + \sigma_u^2\right)$$
$$subject\ to\left|\theta_{g,m}\right|^2 = 1, \forall g, \forall m. \tag{23}$$

After conversion, $\rho = \left[\rho_1, \cdots, \rho_k\right]^T$ does the secondary conversion generate the additional vector. Using the Lagrange multiplier method [29], the optimal solution of ρ_k is shown in formula (26):

$$2\sqrt{\overline{\alpha}_k}\widetilde{\theta}^H\widetilde{v}_{k,k} - 2\rho_k\left(\sum_{j=1}^{K}\left|\widetilde{\theta}^H\widetilde{v}_{k,j}\right|^2 + \sigma_u^2\right) = 0. \tag{24}$$

$$\rho_k\left(\sum_{j=1}^{K}\left|\widetilde{\theta}^H\widetilde{v}_{k,j}\right|^2 + \sigma_u^2\right) = \sqrt{\overline{\alpha}_k}\widetilde{\theta}^H\widetilde{v}_{k,k}. \tag{25}$$

$$\widehat{\rho}_k = \frac{\sqrt{\overline{\alpha}_k}\widetilde{\theta}^H\widetilde{v}_{k,k}}{\sum_{j=1}^{K}\left|\widetilde{\theta}^H\widetilde{v}_{k,j}\right|^2 + \sigma_u^2}. \tag{26}$$

Finally, regarding the complete algorithm, the steps are as follows:

1. Set the initial value variables P and Φ_g.
2. Use Eqs. (16) and (21) to find β_k and p_k, respectively.
3. Using Eqs. (20) and (21) to construct Θ and $V_{k,j}$.
4. Use Eq. (26) to find ρ_k.
5. Output PandΦ_g.
6. Based on the parameters we deduced earlier, we can use pushback to find w_k and v_k as follows:

$$w_k = \frac{1}{\sqrt{2}}\sqrt{\overline{\alpha}_k}\beta_k\Bigg(\underbrace{\mu I_N + \sum_{i=1}^{k}\left|\beta_i\right|^2\tilde{h}_i\tilde{h}_i^H}_{A_1}\Bigg)^{-1}\tilde{h}_k = \frac{1}{\sqrt{2}}\sqrt{\overline{\alpha}_k}\beta_k A_1^{-1}\tilde{h}_k. \tag{27}$$

$$v_k = \frac{1}{\sqrt{2}}\sqrt{\overline{\alpha}_k}\beta_k\Bigg(\underbrace{\mu I_N + \sum_{i=1}^{k}\left|\beta_i\right|^2\tilde{h}_i\tilde{h}_i^H + \sum_{i=1}^{k}\left|\beta_i\right|^2\tilde{e}_i\tilde{e}_i^H}_{A_2}\Bigg)^{-1}\left(\tilde{h}_k + \tilde{e}_k\right)$$
$$= \frac{1}{\sqrt{2}}\sqrt{\overline{\alpha}_k}A_2^{-1}\beta_k\left(\tilde{h}_k + \tilde{e}_k\right). \tag{28}$$

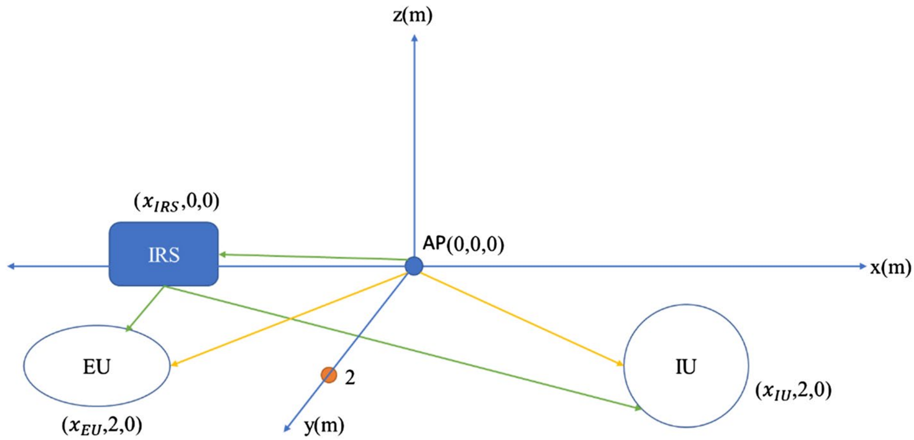

Fig. 2 Simulation Schematic

Table 1 Simulation parameters

Case Parameter	Case I	Case II
Number of users	$K = \{2, 3, 5\}$	
Number of antennae	$N = \{16, 32, 64\}$	$N = \{16, 32\}$
Number of reflecting element	$M = \{5, 10, 15, 20, 25, 30, 35\}$	
Transmitting power (dBm)	$P = \{10, 20, 30, 40, 50, 60, 70\}$	
Channel AP-RIS, AP-EU, AP-IU, RIS-EU, RIS-IU	Raleigh	
Energy harvest power	2×10^{-4}(W)	
x_{IRS}	30 (m)	
Weight	$z_k = 1$	
Number of RIS	1	
x_{IU}	100 (m)	30 (m)
x_{EU}	30 (m)	30 (m)

4 Simulation Results

This section presents the results of the Monte Carlo simulation to validate the effectiveness of the proposed method for the RIS-aided MIMO SWIPT system under different scenarios. The simulation parameters include the number of users (K), the number of antennas (N), the number of reflective elements (M), and the transmission power (P). For the channel part, we use the Rayleigh channel. Figure 2 is a schematic diagram of the simulation environment. Please refer to Case I and II conditions in Table 1 for the simulation parameters setting.

Figure 3 compares the sum-rate obtained by the proposed approach with or without employing RISs corresponding to the Case I condition: two users (information receiving end and energy receiving end), sixteen antennas, and twenty reflective elements, i.e., $K = 2$, $N = 16.$, and $M = 20$. It can be observed from Fig. 3 that with or without employing RISs,

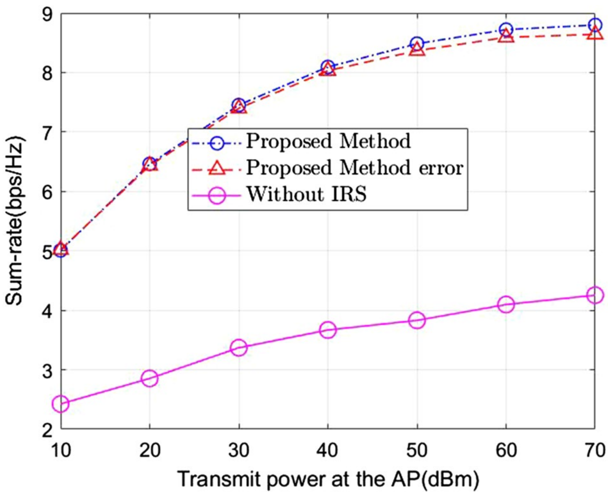

Fig. 3 The sum-rate against transmit power at the AP comparison in Case I condition with scenario: $K=2$, $N=16$, and $M=20$

the sum-rate increases as the transmit power at the AP increases. The curve of the proposed method with a 10% error is approximately the same as the proposed method. The sum-rate performance of the proposed method is higher than the system without employing RISs. The sum-rate improvement is approximately 2 (bps/Hz) and 4 (bps/Hz), corresponding to the transmit power at AP are 10 (dBm) and 70 (dBm), respectively.

Figure 4 compares the sum-rate obtained by the proposed approach with or without employing RISs corresponding to the Case I condition: three users (information receiving end and energy receiving end), sixteen antennas, and twenty reflective elements, i.e., $K=3$, $N=16$., and $M=20$. It can be observed from Fig. 4 that with or without employing RISs, the sum-rate increases as the transmit power at the AP increases. The curve of the proposed method with a 10% error is approximately the same as the proposed method. The sum-rate performance of the proposed method is higher than the system without employing RISs. The sum-rate improvement is approximately 2 (bps/Hz) and 4 (bps/Hz), corresponding to the transmit power at AP are 10 (dBm) and 70 (dBm), respectively. Compared with

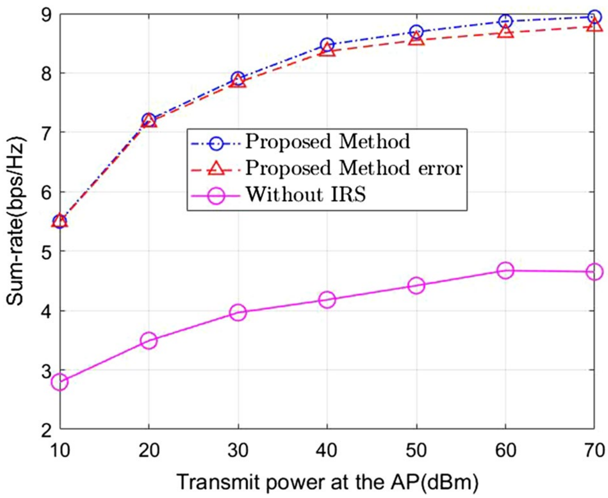

Fig. 4 The sum-rate against transmit power at the AP comparison in Case I condition with scenario: $K=3$, $N=16$, and $M=20$

Fig. 3, the sum-rate also increased by approximately 0.5 (bps/Hs) as the number of users increased.

Figure 5 compares the sum-rate obtained by the proposed approach with or without employing RISs corresponding to the Case I condition: five users (information receiving end and energy receiving end), sixteen antennas, and twenty reflective elements, i.e., $K=5$, $N=16$., and $M=20$. It can be observed from Fig. 5 that with or without employing RISs, the sum-rate increases as the transmit power at the AP increases. The curve of the proposed method with 10% error is approximately the same as the proposed method. The sum-rate performance of the proposed method is higher than the system without employing RISs. The sum-rate improvement is approximately 2 (bps/Hz) and 4 (bps/Hz), corresponding to the transmit power at AP are 10 (dBm), and 70 (dBm), respectively. Compared with Fig. 4, the sum-rate also increased by approximately 0.5 (bps/Hs) as the number of users increased.

Figure 6 compares the sum-rate obtained by the proposed approach with or without employing RISs corresponding to the Case I condition: two users (information receiving end and energy receiving end), thirty-two antennas, and twenty reflective elements, i.e., $K=2$, $N=32$, and $M=20$. It can be observed from Fig. 6 that with or without employing RISs, the sum-rate increases as the transmit power at the AP increases. The curve of the proposed method with 10% error is approximately the same as the proposed method. The sum-rate performance of the proposed method is higher than the system without employing RISs. The sum-rate improvement is approximately 2 (bps/Hz) and 4 (bps/Hz), corresponding to the transmit power at AP are 10 (dBm) and 70 (dBm), respectively. Compared with Fig. 3, the sum-rate also increased by approximately 0.5 (bps/Hs) as the number of antennae increased.

Figure 7 compares the sum-rate obtained by the proposed approach with or without employing RISs corresponding to the Case I condition: two users (information receiving end and energy receiving end), sixty-four antennas, and twenty reflective elements, i.e., $K=2$, $N=64$., and $M=20$. It can be observed from Fig. 7 that with or without employing RISs, the sum-rate increases as the transmit power at the AP increases. The curve of the proposed method with 10% error is approximately the same as the proposed method. The sum-rate performance of the proposed method is higher than the system without employing

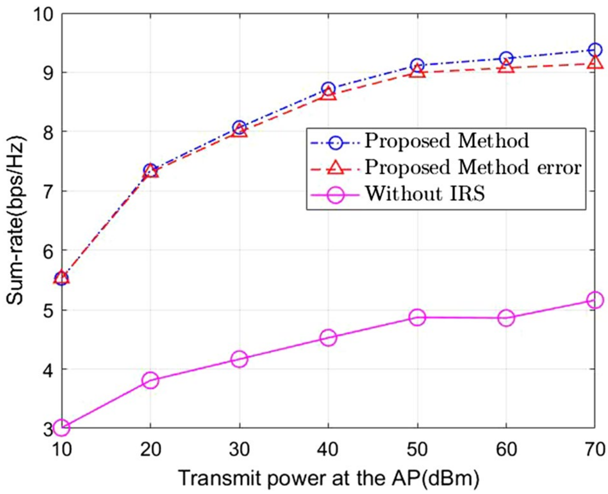

Fig. 5 The sum-rate against transmit power at the AP comparison in Case I condition with scenario: $K=5$, $N=16$, and $M=20$

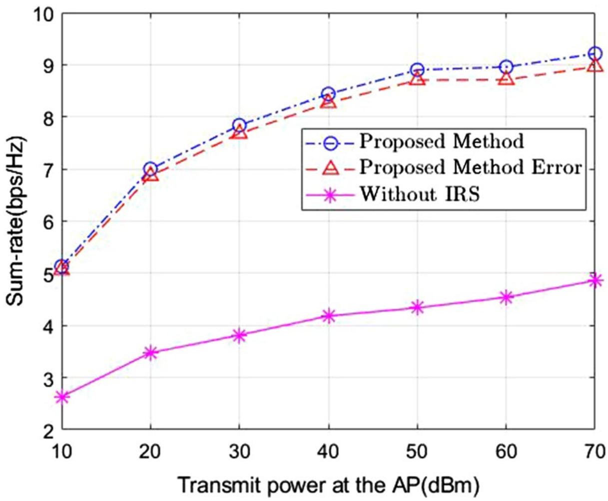

Fig. 6 The sum-rate against transmit power at the AP comparison in Case I condition with scenario: $K=2$, $N=32$, and $M=20$

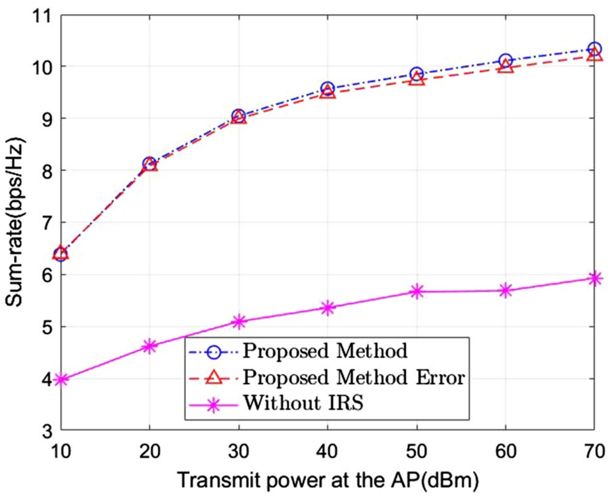

Fig. 7 The sum-rate against transmit power at the AP comparison in Case I condition with scenario: $K=2$, $N=64$, and $M=20$

RISs. The sum-rate improvement is approximately 2 (bps/Hz) and 4 (bps/Hz), corresponding to the transmit power at AP are 10 (dBm) and 70 (dBm), respectively. Compared with Fig. 6, the sum-rate also increased by approximately 1 (bps/Hs) as the number of antennae increased. It can be seen that the influence of the number of antennas on the transmission rate.

Figure 8 compares the sum-rate obtained by the proposed approach with or without employing RISs corresponding to the Case I condition: five users (information receiving end and energy receiving end), sixty-four antennas, and twenty reflective elements, i.e., $K=5$, $N=64$, and $M=20$. It can be observed from Fig. 8 that with or without employing RISs, the sum-rate increases as the transmit power at the AP increases. The curve of the proposed method with a 10% error is approximately the same as the proposed method. The sum-rate performance of the proposed method is higher than the system without employing RISs. The sum-rate improvement is approximately 4 (bps/Hz) and 6 (bps/Hz),

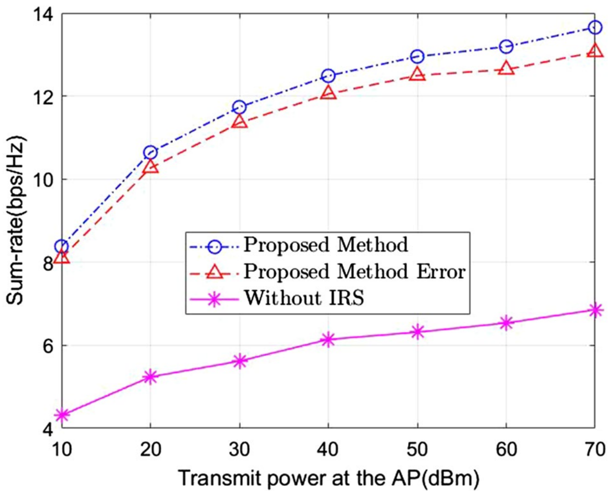

Fig. 8 The sum-rate against transmit power at the AP comparison in Case I condition with scenario: $K = 5$, $N = 64$, and $M = 20$

corresponding to the transmit power at AP are 10 (dBm) and 70 (dBm), respectively. Compared with Fig. 5, the sum-rate also increased by approximately 5 (bps/Hs) as the number of antennae increased. It can be seen that the influence of the number of antennas on the transmission rate.

Figure 9 compares the sum-rate obtained by the proposed approach with or without employing RISs corresponding to the Case I condition: two users (information receiving end and energy receiving end), sixteen antennas, and transmitting power is thirty dBm, i.e., $K = 2$, $N = 16$, and $P = 30$ (dBm). It can be observed from Fig. 9 that when employing RISs, the sum-rate increases as the number of reflecting elements increases. The curve of the proposed method with a 10% error is approximately close to the proposed method. However, the curve of the system without employing RISs remains constant because there are no reflecting elements to aid transmission; hence, the sum-rate will not be enhanced. The sum-rate improvement is approximately 2 (bps/Hz) and 6 (bps/Hz), corresponding to the number of reflecting elements as 5 and 35, respectively.

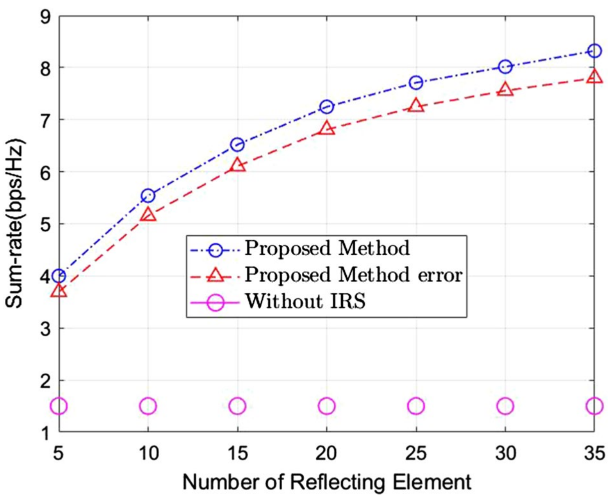

Fig. 9 The sum-rate against the number of reflecting elements comparison in Case I condition with the scenario: $K = 2$, $N = 16$, and $P = 30$ (dBm)

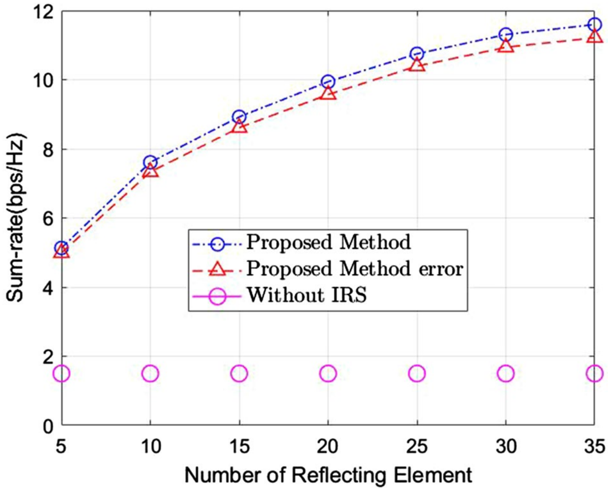

Fig. 10 The sum-rate against the number of reflecting elements comparison in Case I condition with the scenario: $K = 3$, $N = 16$, and $P = 30$ (dBm)

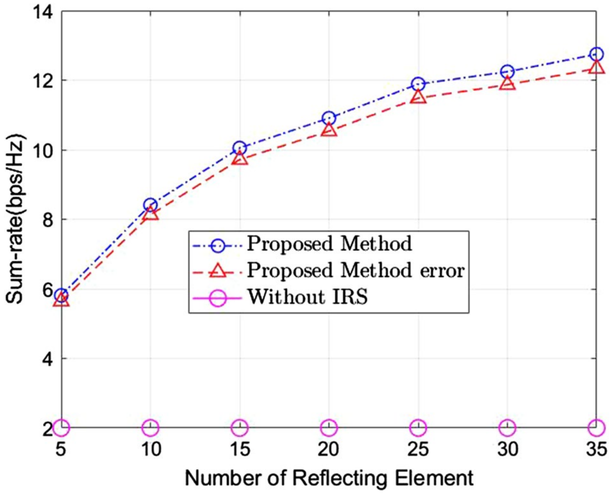

Fig. 11 The sum-rate against the number of reflecting elements comparison in Case I condition with the scenario: $K = 2$, $N = 32$, and $P = 30$ (dBm)

Figure 10 compares the sum-rate obtained by the proposed approach with or without employing RISs corresponding to the Case I condition: three users (information receiving end and energy receiving end), sixteen antennas, and transmitting power is thirty dBm, i.e., $K = 3$, $N = 16$, and $P = 30$ (dBm). It can be observed from Fig. 10 that when employing RISs, the sum-rate increases as the number of reflecting elements increases. The curve of the proposed method with a 10% error is approximately close to the proposed method. However, the curve of the system without employing RISs remains constant because there are no reflecting elements to aid transmission; hence, the sum-rate will not be enhanced. The sum-rate improvement is approximately 3 (bps/Hz) and 10 (bps/Hz), corresponding to the number of reflecting elements as 5 and 35, respectively. Compared with Fig. 9, the sum-rate also increased by approximately 2 (bps/Hs) as the number of reflecting elements is 35.

Figure 11 compares the sum-rate obtained by the proposed approach with or without employing RISs corresponding to the Case I condition: two users (information receiving end and energy receiving end), thirty-two antennas, and transmitting power is thirty dBm, i.e., $K = 2$, $N = 32$, and $P = 30$ (dBm). It can be observed from Fig. 11 that when employing RISs, the sum-rate increases as the number of reflecting elements increases. The curve of the proposed method with a 10% error is approximately close to the proposed method. However, the curve of the system without employing RISs remains constant because there are no reflecting elements to aid transmission; hence, the sum-rate will not be enhanced. The sum-rate improvement is approximately 4 (bps/Hz) and 10 (bps/Hz), corresponding to the number of reflecting elements as 5 and 35, respectively. Compared with Fig. 9, the sum-rate also increased by approximately 4 (bps/Hs) as the number of reflecting elements is 35.

Figure 12 compares the sum-rate obtained by the proposed approach with or without employing RISs corresponding to the Case I condition: three users (information receiving end and energy receiving end), thirty-two antennas, and transmitting power is thirty dBm, i.e., $K = 3$, $N = 64$, and $P = 30$ (dBm). It can be observed from Fig. 12 that when employing RISs, the sum-rate increases as the number of reflecting elements increases. The curve of the proposed method with a 10% error is approximately close to the proposed method. However, the curve of the system without employing RISs remains constant because there are no reflecting elements to aid transmission; hence, the sum-rate will not be enhanced. The sum-rate improvement is approximately 10 (bps/Hz) and 23 (bps/Hz), corresponding to the number of reflecting elements as 5 and 35, respectively. Compared with Fig. 10, the sum-rate also increased by approximately 10 (bps/Hs) as the number of reflecting elements is 35.

Figure 13 compares the sum-rate obtained by the proposed approach with or without employing RISs corresponding to the Case I condition: two users (information receiving end and energy receiving end), thirty-two antennas, and transmitting power is thirty dBm, i.e., $K = 2$, $N = 16$, and $P = 30$ (dBm). It can be observed from Fig. 13 that with or without employing RISs, the sum-rate decreases as the distance increases. Compare the

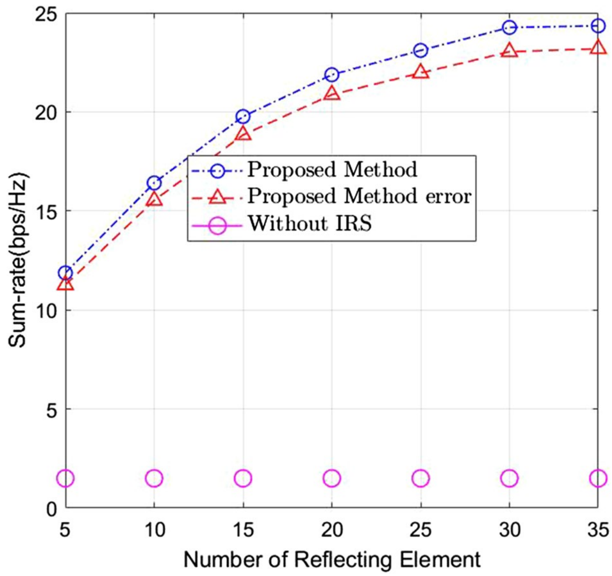

Fig. 12 The sum-rate against the number of reflecting elements comparison in Case I condition with the scenario: $K = 3$, $N = 64$, and $P = 30$ (dBm)

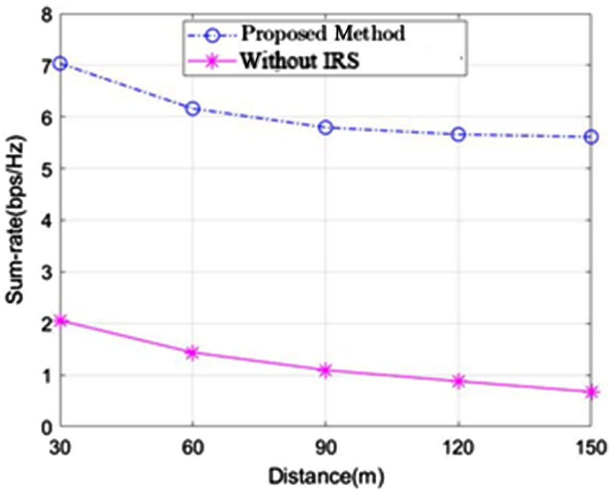

Fig. 13 The sum-rate against the distance comparison in Case I condition with the scenario: $K=2$, $N=16$, and $P=30$ (dBm)

sum-rate at distances 30 (m) and 50 (m), and it drops over 1 (bps/Hz). It can be seen that the influence of the distance on the transmission rate.

Following simulation, the x_{IU} and x_{EU} are set as 30 (m) and 100 (m), respectively. Other parameters remain unchanged. Please refer to Case II in Table 1 for the simulation parameters setting.

Figure 14 compares the sum-rate obtained by the proposed approach with or without employing RISs corresponding to the Case II condition: two users (information receiving end and energy receiving end), sixteen antennas, and twenty reflective elements, i.e., $K=2$, $N=16$., and $M=20$. It can be observed from Fig. 14 that with or without employing RISs, the sum-rate increases as the transmit power at the AP increases. The curve of the proposed method with a 10% error is approximately the same as the proposed method. The sum-rate performance of the proposed method is higher than the system without employing RISs. The sum-rate improvement is approximately 2 (bps/Hz) and

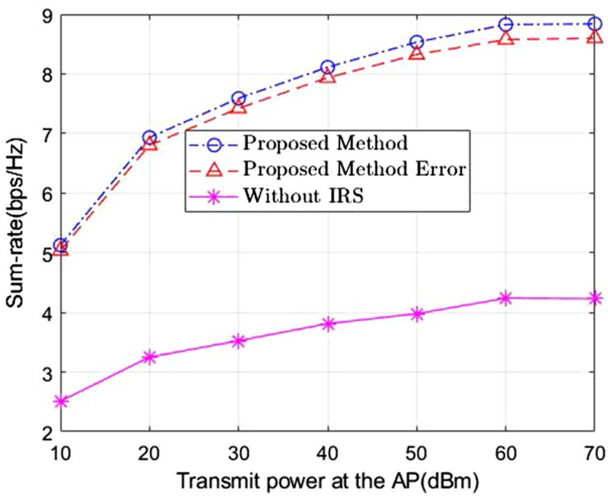

Fig. 14 The sum-rate against transmit power at the AP comparison in Case II condition with scenario: $K=2$, $N=16$, and $M=20$

4 (bps/Hz), corresponding to the transmit power at AP are 10 (dBm) and 70 (dBm), respectively. Compared with Fig. 3, the sum-rate curves are similar.

Figure 15 compares the sum-rate obtained by the proposed approach with or without employing RISs corresponding to the Case II condition: three users (information receiving end and energy receiving end), sixteen antennas, and twenty reflective elements, i.e., $K=3$, $N=16$., and $M=20$. It can be observed from Fig. 15 that with or without employing RISs, the sum-rate increases as the transmit power at the AP increases. The curve of the proposed method with a 10% error is approximately the same as the proposed method. The sum-rate performance of the proposed method is higher than the system without employing RISs. The sum-rate improvement is approximately 2 (bps/Hz) and 4 (bps/Hz), corresponding to the transmit power at AP are 10 (dBm) and 70 (dBm), respectively. Compared with Fig. 4, the sum-rate curves are similar. Compared with Fig. 14, the sum-rate also increased as the number of users increased.

Figure 16 compares the sum-rate obtained by the proposed approach with or without employing RISs corresponding to the Case II condition: five users (information receiving end and energy receiving end), sixteen antennas, and twenty reflective elements, i.e., $K=5$, $N=16$., and $M=20$. It can be observed from Fig. 16 that with or without employing RISs, the sum-rate increases as the transmit power at the AP increases. The curve of the proposed method with a 10% error is approximately the same as the proposed method. The sum-rate performance of the proposed method is higher than the system without employing RISs. The sum-rate improvement is approximately 2 (bps/Hz) and 4 (bps/Hz), corresponding to the transmit power at AP are 10 (dBm) and 70 (dBm), respectively. Compared with Fig. 5, the sum-rate curves are similar. Compared with Fig. 15, the sum-rate also increased as the number of users increased.

Figure 17 compares the sum-rate obtained by the proposed approach with or without employing RISs corresponding to the Case I condition: two users (information receiving end and energy receiving end), thirty-two antennas, and transmitting power is thirty dBm, i.e., $K=2$, $N=32$, and $P=30$ (dBm). It can be observed from Fig. 17 that when employing RISs, the sum-rate increases as the number of reflecting elements increases. The curve

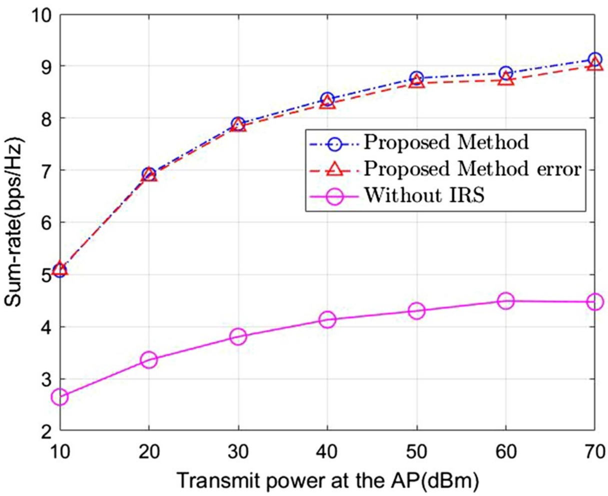

Fig. 15 The sum-rate against transmit power at the AP comparison in Case II condition with scenario: $K=3$, $N=16$, and $M=20$

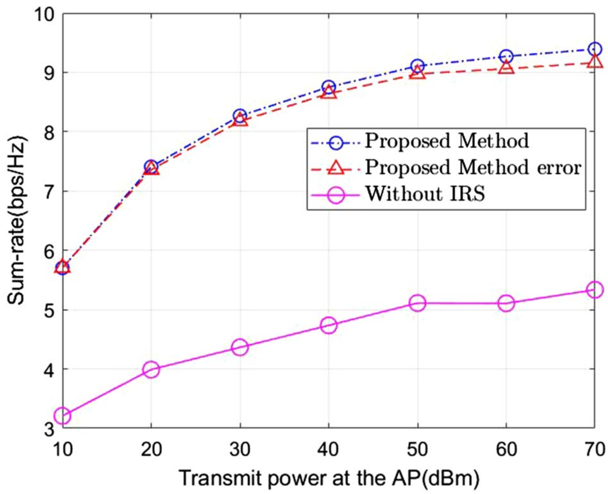

Fig. 16 The sum-rate against transmit power at the AP comparison in Case II condition with scenario: $K=5$, $N=16$, and $M=20$

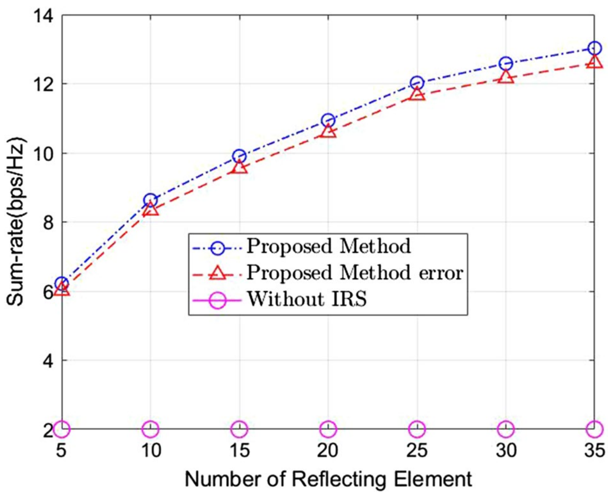

Fig. 17 The sum-rate against the number of reflecting elements comparison in Case II condition with the scenario: $K=2$, $N=32$, and $P=30$ (dBm)

of the proposed method with a 10% error is approximately close to the proposed method. However, the curve of the system without employing RISs remains constant because there are no reflecting elements to aid transmission; hence, the sum-rate will not be enhanced. Compared with Fig. 11, the sum-rate curves are similar.

Table 2 is the simulation summary.

Table 2 Simulation summary

Simulation Scenarios	Sum-rate comparisons
• $K=2,3,5$; $N=16$; $M=20$ (Fig. 3 to Fig. 5)	• The sum-rate of the proposed method is higher than the system without employing RISs • The sum-rate of the proposed method slightly improved as the number of users increased
• $K=5$; $N=16$, 64; $M=20$ (Fig. 5 and Fig. 8) • $K=2$; $N=32$, 64; $M=20$ (Fig. 6 and Fig. 7)	• The sum-rate of the proposed method is higher than the system without employing RISs • The sum-rate of the proposed method slightly improved as the number of antennas increased
• $K=2,3$; $N=16$; $P=30$ (dBm) (Fig. 9 and Fig. 10)	• The sum-rate of the proposed method is higher than the system without employing RISs • The sum-rate of the proposed method slightly improved as the number of users increased • The system without employing RISs remains constant because there are no reflecting elements to aid transmission
• $K=2$; $N=16$, 32; $P=30$ (dBm) (Fig. 9 and Fig. 11) • $K=3$; $N=16$, 64; $P=30$ (dBm) (Fig. 10 and Fig. 12)	• The sum-rate of the proposed method is higher than the system without employing RISs • The sum-rate of the proposed method slightly improved as the number of antennas increased
• Distance (From 30 (m to 150 m) (Fig. 13)	• The sum-rate of the proposed method is higher than the system without employing RISs • The sum-rate decreases as the distance increases with or without employing RISs
• $K=2,3,5$; $N=16$; $M=20$ (Fig. 14 to Fig. 15) • The x_{IU} and x_{EU} are set as 30(m) and 100(m), respectively	• The sum-rate of the proposed method is higher than the system without employing RISs • The sum-rate of the proposed method slightly improved as the number of users increased
• $K=2$; $N=32$; $P=30$ (dBm) (Fig. 17) • The x_{IU} and x_{EU} are set as 30(m) and 100(m), respectively	• The sum-rate of the proposed method is higher than the system without employing RISs • The system without employing RISs remains constant because there are no reflecting elements to aid transmission

5 Conclusion

In this paper, we have studied a new method to improve the performance of a SWIPT communication system by taking advantage of the deployment of RISs. We have formulated the sum-rate maximization problem for the communication system by optimizing subject to the restrictions of the transmission power and the energy harvesting to make the best use of the sum-rate. The simulation outcomes verified the efficiency and effectiveness of the proposed approach.

Author Contributions All authors contributed to the study conception and design. The first draft of the manuscript was written by Fang-Biau Ueng and all authors commented on previous versions of the manuscript. All authors read and approved the final manuscript.

Funding The authors declare that no funds, grants, or other support were received during the preparation of this manuscript.

Data Availability The datasets generated during and/or analysed during the current study are available from the corresponding author on reasonable request.

Declarations

Conflict of interest The authors have no relevant financial or non-financial interests to disclose.

Bibliography

1. Buzzi, S., Chih-Lin, I., Klein, T. E., Poor, H. V., Yang, C., & Zappone, A. (2016). A survey of energy-efficient techniques for 5G networks and challenges ahead. *IEEE Journal on Selected Areas in Communications, 34*(4), 697–709.
2. Sahoo, B. P. S., Chou, C., Weng, C., & Wei, H. (2019). Enabling millimeterwave 5G networks for massive IoT applications: A closer look at the issues impacting millimeter-waves in consumer devices under the 5G framework. *IEEE Consumer Electronics Magazine, 8*(1), 49–54.
3. Kolawole, O. Y., Biswas, S., Singh, K., & Ratnarajah, T. (2020). Transceiver design for energy-efficiency maximization in mmWave MIMO IoT networks. *IEEE Transactions on Green Communications and Networking, 4*(1), 109–123.
4. di Renzo, M., et al. (2020). Smart radio environments empowered by reconfigurable intelligent surfaces: How it works, state of research, and road ahead. [Online]. Available: https://arxiv.org/abs/2004.09352
5. Renzo, M. D., Debbah, M., Phan-Huy, D. T., et al. (2019). Smart radio environments empowered by reconfigurable AI metasurfaces: An idea whose time has come. *Eurasip Journal on Wireless Communications and Networking, 129*.
6. Mursia, P., Sciancalepore, V., Garcia-Saavedra, A., Cottatellucci, L., Pérez, X. C., & Gesbert, D. (2021). RISMA: reconfigurable intelligent surfaces enabling beamforming for IoT massive access. *IEEE Journal on Selected Areas in Communications, 39*(4), 1072–1085.
7. Tan, X., Sun, Z., Jornet, J. M., & Pados, D. (2016, May). Increasing indoor spectrum sharing capacity using smart reflect-array. In *Proceedings of the IEEE international conference on communications (ICC)*, Kuala Lumpur, Malaysia.
8. Li, Y., Jiang, M., Zhang, Q., & Qin, J. (2021). Joint beamforming design in multi-cluster MISO NOMA reconfigurable intelligent surface-aided downlink communication networks. *IEEE Transactions on Communications, 69*(1), 664–674.
9. Basar, E., Di Renzo, M., De Rosny, J., Debbah, M., Alouini, M., & Zhang, R. (2019). Wireless communications through reconfigurable intelligent surfaces. *IEEE Access, 7*, 116753–116773.
10. Basar, E. (2019, June). Transmission through large intelligent surfaces: A new frontier in wireless communications. In *Proceedings of the IEEE European conference on networks and communications (EuCNC)*, Valencia, Spain.
11. Özdogan, Ö., Björnson, E., & Larsson, E. G. (2020). Intelligent reflecting surfaces: Physics, propagation, and pathloss modeling. *IEEE Wireless Communications Letters, 9*(5), 581–585.
12. Tang, W., Chen, M. Z., Chen, X., Dai, J. Y., Han, Y., Di Renzo, M., et al. (2021). Wireless communications with reconfigurable intelligent surface: Path loss modeling and experimental measurement. *IEEE Transactions on Wireless Communications*, *20*(1), 421–439.
13. Hu, S., Rusek, F., & Edfors, O. (2018). Beyond massive MIMO: The potential of positioning with large intelligent surfaces. *IEEE Transactions on Signal Processing, 66*(7), 1761–1774.
14. Zhang, S., & Zhang, R. (2020). Capacity characterization for intelligent reflecting surface aided MIMO communication. *IEEE Journal on Selected Areas in Communications*, *38*(8), 1823–1838.
15. Cui, M., Zhang, G., & Zhang, R. (2019, December). Secure wireless communication via intelligent reflecting surface. In *Proceedings of the IEEE Global Communications Conference (GLOBECOM)*, Waikoloa, HI, USA.
16. Yu, X., Xu, D., Sun, Y., Ng, D. W. K., & Schober, R. (2020). Robust and secure wireless communications via intelligent reflecting surfaces. *IEEE Journal on Selected Areas in Communications, 38*, 2637.
17. Fu, M., Zhou, Y., & Shi, Y. (2019). Intelligent reflecting surface for downlink non-orthogonal multiple access networks. In *IEEE Globecom workshops (GC Wkshps)* (pp. 1–6).
18. Jiang, T., & Shi, Y. (2019). Over-the-air computation via intelligent reflecting surfaces. In *IEEE global communications conference* (GLOBECOM) (pp. 1–6).

19. Huang, C., et al. (2018, December). Energy efficient multiuser MISO communication using low resolution large intelligent surfaces. In *Proceedings of the IEEE Globecom workshops (GC WKSHPS)*, Abu Dhabi, United Arab Emirates.
20. Huang, C., Zappone, A., Alexandropoulos, G. C., Debbah, M., & Yuen, C. (2019). Reconfigurable intelligent surfaces for energy efficiency in wireless communication. *IEEE Transactions on Wireless Communications, 18*, 4157–4170.
21. Huang, C., et al. (2019). Holographic MIMO surfaces for 6G wireless networks: Opportunities, challenges, and trends. [Online]. Available: http://arxiv.org/abs/1911.12296
22. Ntontin, K., et al. (2019). Reconfigurable intelligent surfaces vs. relaying: differences, similarities, and performance comparison. [Online]. Available: http://arxiv.org/abs/1908.08747
23. Björnson, E., & Sanguinetti L. (2019). Demystifying the power scaling law of intelligent reflecting surfaces and metasurfaces. In *IEEE 8th international workshop on computational advances in multi-sensor adaptive processing (CAMSAP)*.
24. Ntontin, K., Song, J., Renzo, M. D., & Member, S. (2019). Multi-antenna relaying and reconfigurable intelligent surfaces: Endto-End SNR and achievable rate. [Online]. Available: http://arxiv.org/abs/1908.07967
25. Björnson, E., Özdogan, Ö., & Larsson, E. G. (2019). Intelligent reflecting surface vs. decode-and-forward: How large surfaces are needed to beat relaying? [Online]. Available: http://arxiv.org/abs/1906.03949
26. Hu, J., Liang, Y.-C., & Pei, Y. (2021). Reconfigurable intelligent surface enhanced multiuser MISO symbiotic radio system. *IEEE Transactions on Communications, 69*(4), 2359–2371. https://doi.org/10.1109/TCOMM.2020.3047444
27. Lu, L., Li, G. Y., Swindlehurst, A. L., Ashikhmin, A., & Zhang, R. (2014). An overview of massive MIMO: Benefits and challenges. *IEEE Journal on Selected Topics in Signal Processing, 8*(5), 742–758.
28. Liu, H., Hu, F., Qu, S., et al. (2019). Multipoint wireless information and power transfer to maximize sum-throughput in WBAN with energy harvesting. *IEEE Internet of Things Journal, 6*(4), 7069–7078.
29. Varga, L. O., Romaniello, G., Vucinic, M., et al. (2015). Greennet: An energy-harvesting IP-enabled wireless sensor network. *IEEE Internet Things Journal, 2*(5), 412–426.
30. Yu, G., Chen, X., Zhong, C., et al. (2020). Design, analysis and optimization of a large intelligent reflecting surface aided B5G cellular Internet of Things. *IEEE Internet Things Journal, 7*, 8902.
31. Wu, Q., & Zhang, R. (2019). Towards smart and reconfigurable environment: Intelligent reflecting surface aided wireless network. *IEEE Communications Magazine, 58*(1), 106–112.
32. Wu, Q., & Zhang, R. (2019). Intelligent reflecting surface enhanced wireless network via joint active and passive beamforming. *IEEE Transactions on Wireless Communications, 18*(11), 5394–5409.
33. Gong, S., Yang, Z., Xing, C., An, J., & Hanzo, L. (2021). Beamforming optimization for intelligent reflecting surface aided SWIPT IoT networks relying on discrete phase shifts. *IEEE Internet of Things Journal, 8*(10), 8585–8602. https://doi.org/10.1109/JIOT.2020.3046929
34. Zhang, S., & Zhang, R. (2020). Capacity characterization for intelligent reflecting surface aided MIMO communication. *IEEE Journal on Selected Areas in Communications, 38*, 1823.
35. Pan, C., Ren, H., Wang, K., Xu, W., Elkashlan, M., Nallanathan, A., & Hanzo, L. (2019). Intelligent reflecting surface for multicell MIMO communications, arXiv preprint arXiv:1907.10864.
36. Yang, Y., Zheng, B., Zhang, S., & Zhang, R. (2020). Intelligent reflecting surface meets OFDM: Protocol design and rate maximization. *IEEE Transactions on Communications, 68*(7), 4522–4535.
37. Zheng, B., & Zhang, R. (2020). Intelligent reflecting surface-enhanced OFDM: Channel estimation and reflection optimization. *IEEE Wireless Communications Letters, 9*(4), 518–522.
38. He, Z. Q., & Yuan, X. (2020). Cascaded channel estimation for large intelligent metasurface assisted massive MIMO. *IEEE Wireless Communications Letters, 9*, 210.
39. You, C., Zheng, B., & Zhang, R. (2019). Progressive channel estimation and passive beamforming for intelligent reflecting surface with discrete phase shifts, arXiv preprint arXiv:1912.10646.
40. Lu, X., Wang, P., Niyato, D., Kim, D. I., & Han, Z. (2014). Wireless networks with RF energy harvesting: A contemporary survey. *IEEE Commun. Surveys Tuts., 17*(2), 757–789.
41. Huang, Y., Liu, M., & Liu, Y. (2018). Energy-efficient SWIPT in IoT distributed antenna systems. *IEEE Internet of Things Journal, 5*(4), 2646–2656.
42. Chae, S. H., Jeong, C., & Lim, S. H. (2018). Simultaneous wireless information and power transfer for Internet of Things sensor networks. *IEEE Internet of Things Journal, 5*(4), 2829–2843.
43. Wu, Q., & Zhang, R. (2020). Weighted sum power maximization for intelligent reflecting surface aided SWIPT. *IEEE Wireless Communications Letters, 9*(5), 586–590.
44. Tang, Y., Ma, G., Xie, H., Xu, J., & Han, X. (2019). Joint transmit and reflective beamforming design for IRS-assisted multiuser MISO SWIPT systems, arXiv preprint arXiv:1910.07156.

45. Wu, Q., & Zhang, R. (2019). Joint active and passive beamforming optimization for intelligent reflecting surface assisted SWIPT under QoS constraints, arXiv preprint arXiv:1910.06220.
46. Mu, X., Liu, Y., Guo, L., Lin, J., & Al-Dhahir, N. (2019). Exploiting intelligent reflecting surfaces in multi-antenna aided NOMA systems, arXiv preprint arXiv:1910.13636.
47. Zheng, B., Wu, Q., & Zhang, R. (2020). Intelligent reflecting surface-assisted multiple access with user pairing: NOMA or OMA? *IEEE Communications Letters, 24*(4), 753–757.
48. Guan, X., Wu, Q., & Zhang, R. (2020). Intelligent reflecting surface assisted secrecy communication: Is artificial noise helpful or not? *IEEE Wireless Communications Letters, 9*(6), 778–782.
49. Cui, M., Zhang, G., & Zhang, R. (2019). Secure wireless communication via intelligent reflecting surface. *IEEE Wireless Commun. Lett., 8*(5), 1410–1414.
50. Wu, Q., & Zhang, R. (2020). Beamforming optimization for wireless network aided by intelligent reflecting surface with discrete phase shifts. *IEEE Transactions on Communications*, *68*(3), 1838–1851.

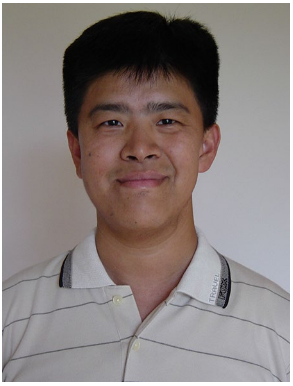

Fang-Biau Ueng received the Ph.D. degree in electronic engineering from the National Chiao Tung UniversityHsinchu, Taiwan in 1995. From 1996 to 2001 he was with National Space Program Office (NSPO) of Taiwan as an associate researcher. From 2001 to 2002 he was with Siemens Telecommunication Systems Limited (STSL), Taipei, Taiwan, where he was involved in the design of mobile communication systems. Since February 2002 he has been with the department of electrical engineering, National Chung-Hsing UniversityTaichung, Taiwan. His areas of research interest are wireless communication and adaptive signal processing.

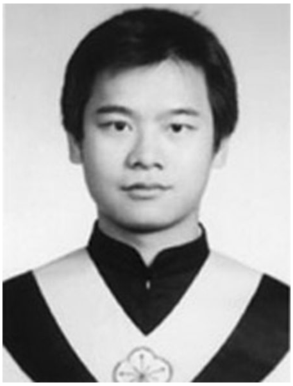

Hsuan-Fu Wang was born in Taipei, Taiwan, R.O.C. in March 1972. He received the B.S. degree in electrical engineering from Chinese Cultural UniversityTaipeiTaiwan, in 1995 and the M.S. degree in space science from National Central UniversityTaoyuan, Taiwanin 1997. From 1995 to 1996, he was with the Alcatel Telecom, Taiwan (Taisel). From 1997 to 1999, he was with the Coast Guard Command, Taiwan. From 1999 to 2003, he was with Mobitai Communications Corp., Taichung, Taiwan. Currently, he is pursuing a Ph. D. degree in the department of electrical engineering of National Chung-Hsing UniversityTaichung, Taiwan. His research interests include microwave remote sensing, radar signal processing and mobile communications.

Huang-Wei Shen was born in Tainan, Taiwan, in 1997. He received the B.Sc. degree in Department of Applied Mathematics from National Chiayi University, Chiayi, Taiwan, in 2019 and the M.Sc. degree in communication engineering from National Chung Hsing University (NCHU), Taichung, Taiwan, in 2022. He was a member of the Communication Systems Laboratory, National Chung Hsing University (NCHU). His research interest is focused on Intelligent Reflecting Surface.